iScience

CellPress
OPEN ACCESS

Article

M2 macrophage-derived exosomal microRNA-411-5p impedes the activation of hepatic stellate cells by targeting CAMSAP1 in NASH model

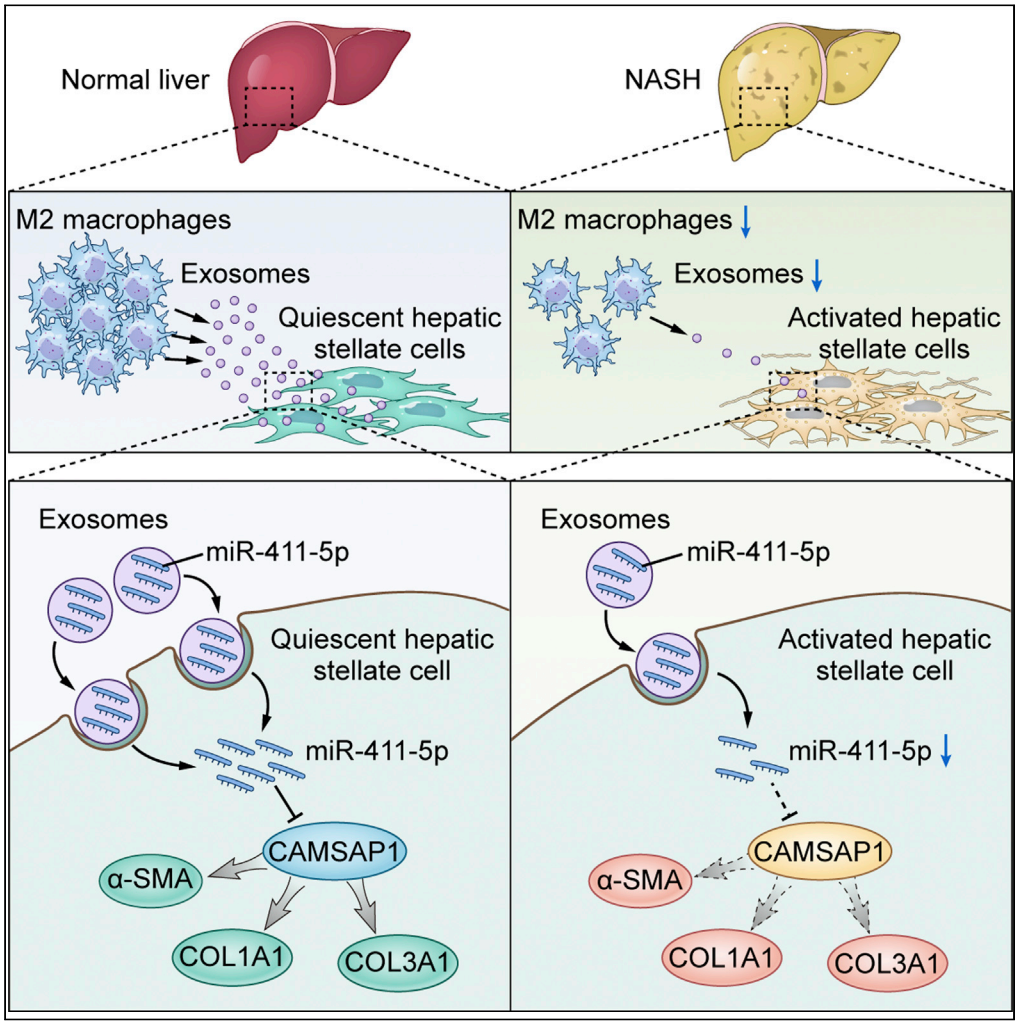

Zhiping Wan, Xiaoan Yang, Xiaoquan Liu, Yinfang Sun, Piaojian Yu, Fen Xu, Hong Deng

xufen3@mail.sysu.edu.cn (F.X.)
dhong@mail.sysu.edu.cn (H.D.)

Highlights

M2 macrophage markers are decreased in the HFHCD-induced rat model of NASH

M2 macrophage-derived exosomes inhibit HSCs activation via miR-411-5p

CAMSAP1 is a direct target of miR-411-5p

Knockdown of CAMSAP1 inhibits HSCs activation

Wan et al., iScience 25, 104597
July 15, 2022
https://doi.org/10.1016/j.isci.2022.104597

iScience

CellPress
OPEN ACCESS

Article

M2 macrophage-derived exosomal microRNA-411-5p impedes the activation of hepatic stellate cells by targeting CAMSAP1 in NASH model

Zhiping Wan,[1,4,5,6] Xiaoan Yang,[1,5,6] Xiaoquan Liu,[1,5] Yinfang Sun,[3] Piaojian Yu,[2,4] Fen Xu,[2,4,*] and Hong Deng[1,5,7,*]

SUMMARY

Liver fibrosis is a severe stage of nonalcoholic fatty liver disease (NAFLD), which is closely associated with the activation of hepatic stellate cells (HSCs) and their interaction with macrophages. Exosomes can mediate crosstalk between macrophages and HSCs in NAFLD-associated fibrosis. We found that M2 macrophage-derived exosomes significantly inhibit HSCs activation. RNA-seq studies revealed that miRNA-411-5p was decreased in serum exosomes of nonalcoholic steatohepatitis (NASH) patients as compared with that in healthy controls. Besides, miR-411-5p and M2 macrophage markers are decreased in the liver of the NASH model. We further proved that exosomal miR-411-5p from M2 macrophages inhibit HSCs activation and miR-411-5p directly downregulated the expression of Calmodulin-Regulated Spectrin-Associated Protein 1 (*CAMSAP1*) to inactivate stellate cells. Importantly, knockdown of *CAMSAP1* also inhibited HSCs activation. This study contributes to understanding the underlying mechanism of HSCs activation and indicates *CAMSAP1* may serve as a potential therapeutic target for NASH.

INTRODUCTION

Nonalcoholic fatty liver disease (NAFLD) is a predominant form of chronic liver disease, affecting nearly 25% of the global population (Diehl and Day, 2017; Younossi et al., 2019). It is characterized by a continuous spectrum of liver diseases, including nonalcoholic simple steatosis (NAFL), nonalcoholic steatohepatitis (NASH), cirrhosis, and ultimately liver cancer (Sheka et al., 2020). The initiation of liver fibrosis is an important pathological change in the course of NASH progression, which is closely related to the activation of hepatic stellate cells (HSCs) and the interaction between HSCs and macrophages (Seki and Schwabe, 2015; Tacke and Zimmermann, 2014).

Macrophage population in the injured liver is composed of hepatic macrophages and monocyte-derived infiltrating macrophages (Gordon and Taylor, 2005). According to the received signals, these macrophages can differentiate into either M1 or M2 macrophages expressing corresponding molecular markers to regulate liver inflammation and fibrosis (Wan et al., 2014). Hepatic macrophages play an important role in the initiation and progression of hepatic fibrosis (Cheng et al., 2021). However, the molecular mechanism responsible for mediating the crosstalk between HSCs and hepatic macrophages, especially the M2 macrophages, is not fully elucidated.

Recently, exosomes have attracted widespread attention from both fundamental and translational researchers. Exosomes are minuscule membrane vesicles with a diameter of about 30–150 nm that are secreted by most cell types (Yanez-Mo et al., 2015). Exosomes mediate intercellular communication by transporting proteins, lipids, and nucleic acids (Kim et al., 2015; Raposo and Stoorvogel, 2013). Thus, the role of exosomes in the initiation and progression of hepatic fibrosis cannot be disregarded.

MicroRNAs (miRNAs) are small noncoding RNAs with a length of about 19-24 nucleotides, which can regulate gene expression by binding to the 3′-UTR region of their target gene (Androvic et al., 2017; Bartel, 2009; Huntzinger and Izaurralde, 2011). miRNAs can be transported to recipient cells by exosomes to regulate the biological functions of recipient cells (Potrich et al., 2017). Exosome-mediated miRNA shuttle is an

[1]Department of Infectious Diseases, the Third Affiliated Hospital, Sun Yat-sen University, Guangzhou 510630, China

[2]Department of Endocrinology and Metabolism, the Third Affiliated Hospital, Sun Yat-sen University, Guangzhou 510630, China

[3]Department of General Intensive Care Unit, the Third Affiliated Hospital, Sun Yat-sen University, Guangzhou 510630, China

[4]Guangdong Provincial Key Laboratory of Diabetology, the Third Affiliated Hospital, Sun Yat-sen University, Guangzhou 510630, China

[5]Guangdong Provincial Key Laboratory of Liver Disease Research, the Third Affiliated Hospital, Sun Yat-sen University, Guangzhou 510630, China

[6]These authors contributed equally

[7]Lead contact

*Correspondence: xufen3@mail.sysu.edu.cn (F.X.), dhong@mail.sysu.edu.cn (H.D.)

https://doi.org/10.1016/j.isci.2022.104597

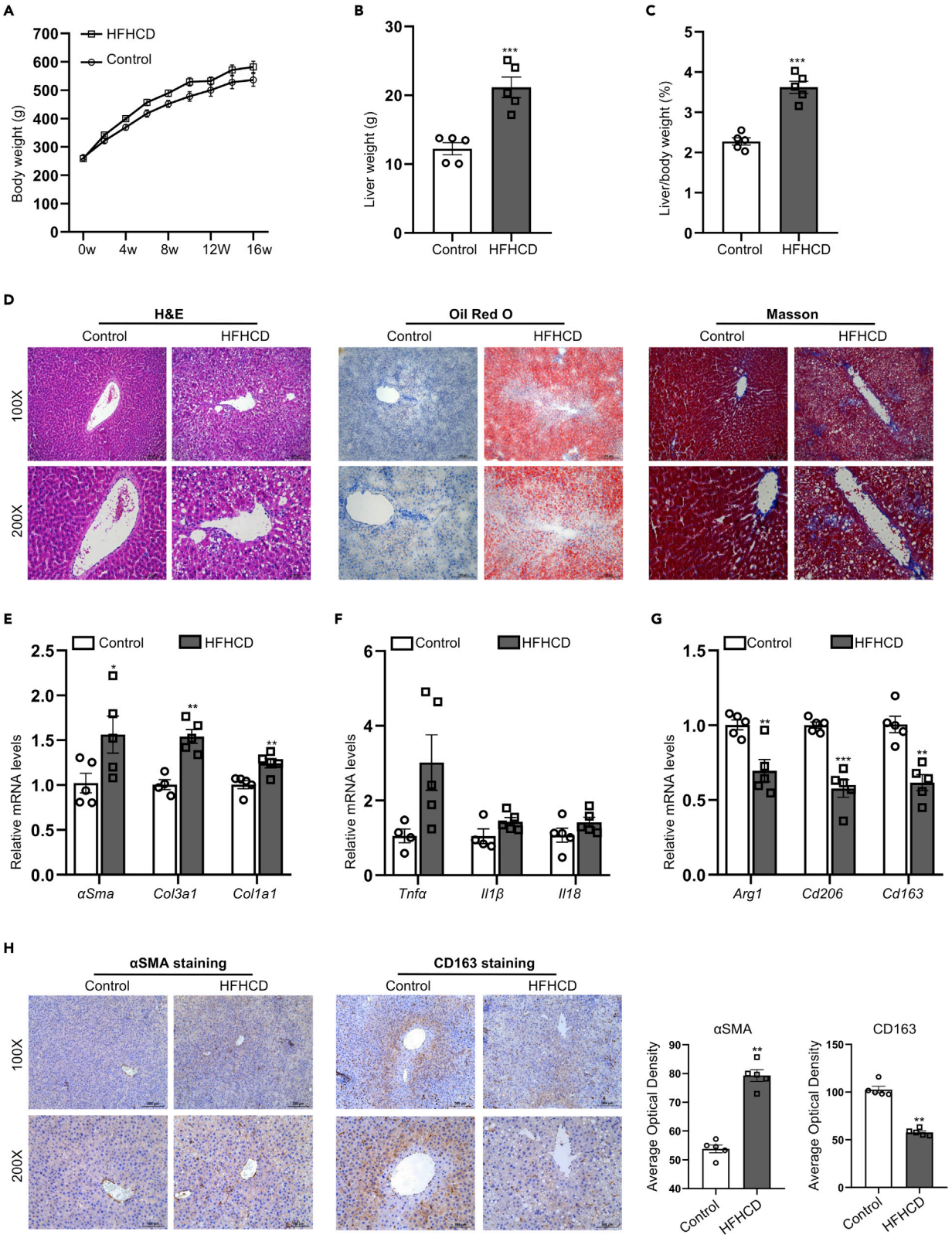
A
HFHCD
Control
Body weight (g)
0w
4w
8w
12W
16w
B
Liver weight (g)
Control
HFHCD
C
Liver/body weight (%)
Control
HFHCD
D
H&E
Oil Red O
Masson
Control
HFHCD
100X
200X
E
Control
HFHCD
Relative mRNA levels
αSma
Col3a1
Col1a1
F
Tnfα
Il1β
Il18
G
Arg1
Cd206
Cd163
H
αSMA staining
CD163 staining
Average Optical Density

Figure 1. M2 macrophage markers are decreased in the HFHCD-induced rat model of NASH

Male Sprague-Dawley rats at 7 weeks of age were fed with a regular chow (Control) or a high-fat high-cholesterol diet (HFHCD) for 16 weeks.

(A–C) Body weight trends, liver weights, and liver/body weight ratios in rats.

(D) The sections of rat livers were stained with H&E, Oil red O, and Masson. Magnifications: 100X (scale bar = 200μm) and 200X (scale bar = 100μm).

(E) The mRNA levels of fibrosis-related genes (*αSma*, *Col1a1*, and *Col3a1*) in rat livers were analyzed by RT-qPCR.

(F) The mRNA levels of M1 macrophage markers (*Tnfα*, *Il1β*, and *Il18*) in rat livers were analyzed by RT-qPCR.

(G) The mRNA levels of M2 macrophage markers (*Arg1*, *Cd206*, and *Cd163*) in rat livers were analyzed by RT-qPCR.

(H) The expression of αSMA (fibrosis-related gene) and CD163 (M2 macrophage marker) in rat livers were analyzed by immunohistochemistry. Magnifications: 100× (scale bar = 200μm) and 200X (scale bar = 100μm). Data are expressed as means ± SEM (n = 4–5). The statistical significance of the difference between two groups was analyzed by Student's *t*-test. *, **and *** represent p values less than 0.05, 0.01, and 0.001, respectively, in comparison to Control groups.

important route of intercellular communication in liver fibrosis progression. Exosomes secreted from quiescent HSCs have been shown to decrease the fibrogenic potential of activated HSCs via miR-214 or miR-199a-5p (Chen et al., 2014, 2016). Natural killer cells-derived exosomes have been reported to inhibit the HSCs activation mediated by miR-223 (Wang et al., 2020). Furthermore, exosomal miR-1297 derived from lipotoxic hepatocytes evidently contributes to the activation and proliferation of HSCs (Luo et al., 2021). Exosomes secreted from activated HSCs stimulate macrophage migration and the production of IL-6 and TNFα (Benbow et al., 2021). In addition, exosomes derived from lipopolysaccharide-stimulated macrophages activate HSCs through miR-103-3p (Chen et al., 2020) and accelerates liver fibrosis through miR-500 (Chen et al., 2021a).

M2 macrophages polarization is closely correlated with the inhibition of HSCs activation and the alleviation of liver fibrosis (Sakai et al., 2020; Su et al., 2021; Yang et al., 2018). However, the crosstalk between M2 macrophages and HSCs and the involvement of exosomes in this process remains unclear. In this study, we aimed to delineate the mechanisms underlying the regulatory role of M2 macrophages in HSCs activation and advance our understanding of the progression of NASH.

RESULTS

M2 macrophage marker expression is decreased in liver tissues of HFHC diet-induced rat model of NASH

To explore the role of hepatic macrophages in progression of NASH, we used a high-fat high-cholesterol diet (HFHCD) fed rat model. Our results revealed that after 16 weeks of feeding, both the liver weight and the liver weight/body weight ratio were significantly increased in the HFHCD group as compared with those in the control group (Figures 1A–1C). Further analysis revealed that the rats fed with HFHCD manifested steatosis, lobular inflammation, and mild fibrosis in the liver as demonstrated by the hematoxylin and eosin (H&E), oil red O, and Masson stainings, respectively (Figure 1D). Subsequently, expression levels of fibrosis-related genes such as α-smooth muscle actin (*αSma*), type I collagen (*Col1a1*), and type III collagen (*Col3a1*) were examined in the rat liver tissues. The mRNA expression of these genes (*αSma*, *col1a1*, and *Col3a1*) was elevated in the liver tissues of HFHCD-fed rats as compared to normal control diet fed rats (Figure 1E). However, the expression of M1 macrophage markers, tumor necrosis factor alpha (*Tnfα*), interleukin-1β (*Il1β*), and interleukin 18 (*Il18*), was not statistically different between the control and HFHCD group (Figure 1F). Interestingly, the expression levels of M2 macrophage markers such as arginase 1 (*Arg1*), *Cd206*, and *Cd163*, were significantly decreased in the livers of rats fed with HFHCD diet as compared with those observed in control group (Figure 1G). We also found that the expression of CD163 was decreased, whereas the expression of αSMA was elevated in the liver tissues of HFHCD fed rats as compared with normal controls indicated by immunohistochemical staining (Figure 1H). Overall, these results suggest that the initiation of liver fibrosis in HFHCD fed rats is accompanied with a decrease of M2 macrophages. Moreover, previous study has shown that the decrease of M2 macrophages precedes the initiation of liver fibrosis (Liu et al., 2020). Consequently, we speculated that M2 macrophages might play an important role in inhibiting the activation of HSCs, which could be potentially mediated by the M2 macrophage-derived exosomes.

Characterization of exosomes derived from M2 macrophages

To collect the exosomes secreted by M2 macrophages, we first differentiated the THP-1 cells into M2 macrophages by stimulating them with IL4 and IL13 (Chanput et al., 2014; Genin et al., 2015). Flow cytometry analysis showed a significant increase in the percentage of $CD206^{+}$ cells in the Il4+Il13 treatment group as compared with that in the control group. Likewise, the expression of *CD206* transcripts in the Il4+Il13

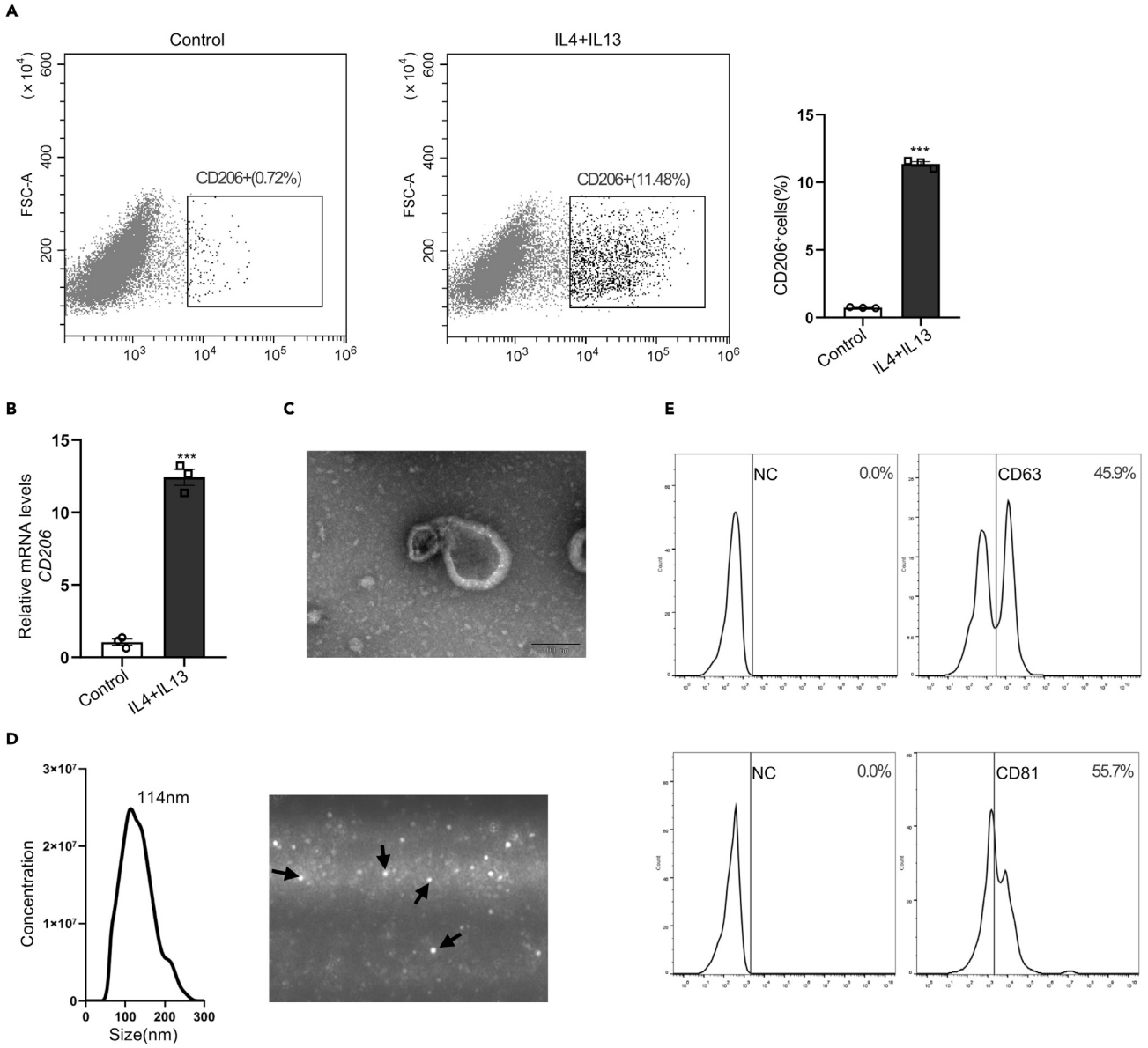

Figure 2. Characterization of exosomes derived from mature M2 macrophages

The THP-1 monocytes were treated with 100 ng/mL PMA for 24 h for differentiation into macrophages. The macrophage M2 polarization was achieved by incubation with 20 ng/mL of IL4 and IL13 for 48 h. The exosomes were then collected from the M2 macrophage culture medium by ultrafiltration.

(A) The percentage of M2 ($CD206^+$) macrophages was estimated by flow cytometry (n = 3).

(B) The mRNA levels of M2 macrophage markers *CD206* were analyzed by RT-qPCR (n = 3).

(C) Representative transmission electron microscopic photographs of M2 macrophage-derived exosomes (scale bar = 100 nm).

(D) M2 macrophage-derived exosomes were investigated by Nanoparticle Tracking Analyses (NTA); the black arrows indicate small particles moving in Brownian motion.

(E) Flow cytometry showing the expression of exosome markers—CD63 and CD81—in M2 macrophage-derived exosomes. Data are expressed as mean ± SEM The statistical significance of the difference between two groups was analyzed by Student's *t*-test. *** denotes $p < 0.001$ in comparison to Control groups.

treatment group was significantly upregulated (Figures 2A and 2B). These results indicate that THP-1 cells were successfully differentiated into M2 macrophages after stimulation with Il4 and Il13. Subsequently, we isolated and identified exosomes secreted by M2 macrophages from the culture medium. The transmission electron microscopy (TEM) and nanoparticle tracking analysis (NTA) studies further revealed that M2 macrophage-derived exosomes exhibited a characteristic cup-shaped structure and an average diameter

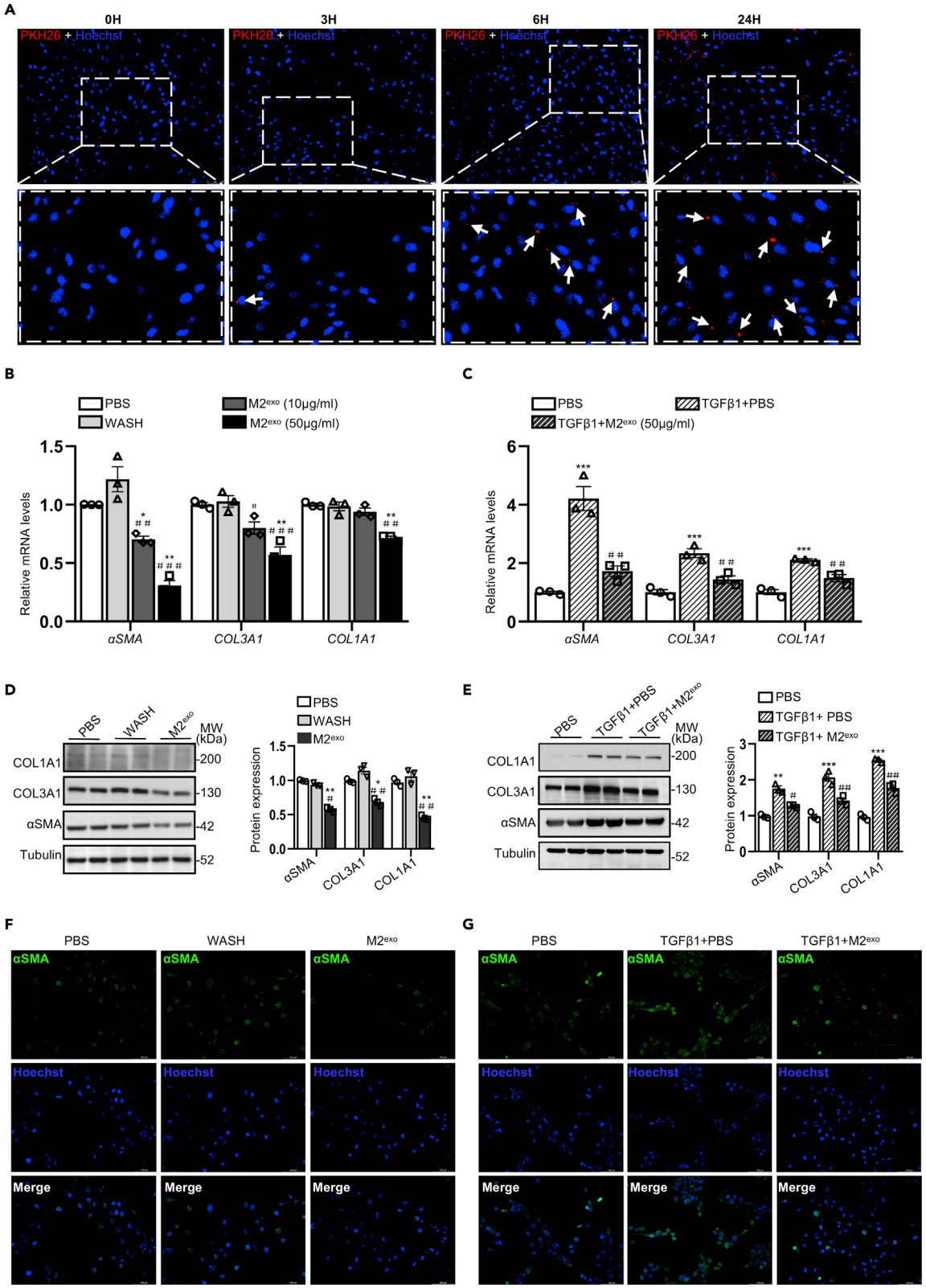
A
0H
3H
6H
24H
PKH26 + Hoechst
B
PBS
WASH
M2exo (10μg/ml)
M2exo (50μg/ml)
Relative mRNA levels
αSMA
COL3A1
COL1A1
C
PBS
TGFβ1+PBS
TGFβ1+M2exo (50μg/ml)
Relative mRNA levels
αSMA
COL3A1
COL1A1
D
PBS
WASH
M2exo
MW (kDa)
COL1A1
COL3A1
αSMA
Tubulin
200
130
42
52
Protein expression
E
PBS
TGFβ1+PBS
TGFβ1+M2exo
MW (kDa)
COL1A1
COL3A1
αSMA
Tubulin
200
130
42
52
Protein expression
TGFβ1+ PBS
TGFβ1+ M2exo
F
PBS
WASH
M2exo
αSMA
Hoechst
Merge
G
PBS
TGFβ1+PBS
TGFβ1+M2exo
αSMA
Hoechst
Merge

Figure 3. M2 macrophage-derived exosomes inhibit HSCs activation

(A) LX2 cells were incubated with PKH26-labeled M2 macrophage-derived exosomes, and the exosomes internalization was observed by an inverted fluorescence microscope. The white arrows indicate PKH26-labeled exosomes (scale bar = 50μm).

(B) The mRNA levels of *αSMA*, *COL1A1*, and *COL3A1* were analyzed by RT-qPCR in LX2 cells treated with PBS, WASH, and M2 macrophage-derived exosomes (10 μg/mL or 50 μg/mL) (n = 3).

(C) The mRNA levels of *αSMA*, *COL1A1*, and *COL3A1* were analyzed by RT-qPCR in TGFβ1-treated LX2 cells treated with M2 macrophage-derived exosomes or PBS (n = 3).

(D) Levels of αSMA, COL1A1, and COL3A1 protein were analyzed by western blotting studies in LX2 cells treated with PBS, WASH, and 50 μg/mL M2 macrophage-derived exosomes (n = 3).

(E) Levels of αSMA, COL1A1, and COL3A1 protein were analyzed by western blotting studies in TGFβ1-treated LX2 cells treated with M2 macrophage-derived exosomes or PBS (n = 3).

(F) Expression of αSMA was analyzed by immunofluorescence staining in LX2 cells treated with PBS, WASH, and 50 μg/mL M2 macrophage-derived exosomes (scale bar = 100μm).

(G) Expression of αSMA was analyzed by immunofluorescence staining in TGFβ1-treated LX2 cells treated with M2 macrophage-derived exosomes or PBS (scale bar = 100μm). WASH is PBS obtained after washing exosomes twice; $M2^{exo}$: M2 macrophage-derived exosomes. Data are expressed as mean ± SEM The statistical significance of the difference between the compared groups was analyzed by one-way ANOVA. *, **and ***denotes p values less than 0.05, 0.01, and 0.001, respectively, in comparison to PBS groups; whereas $^{\#}$, $^{\#\#}$, and $^{\#\#\#}$ represent p values less than 0.05, 0.01, and 0.001, respectively, in comparison to WASH groups or TGFβ1+PBS groups.

of 114 nm (Figures 2C and 2D). In addition, flow cytometry analysis revealed that the expression levels of exosomal surface markers CD63 and CD81 were 45.9% and 55.7%, respectively (Figure 2E). Collectively, we successfully isolated and purified exosomes secreted by M2 macrophages.

M2 macrophage-derived exosomes inhibit HSCs activation

To investigate the role of exosomes secreted by M2 macrophages in the interaction between M2 macrophages and HSCs in the progression of NASH, we firstly examined if the M2 macrophage-derived exosomes ($M2^{exo}$) could be taken up by HSCs. Consequently, we labeled the exosomes secreted by M2 macrophages with PKH26 (a red fluorescent dye). After treatment with PKH26-labeled exosomes for 6 h, the red fluorescence clearly appeared within HSCs (Figure 3A). Besides, the fluorescence was increased at 24 h after treatment, revealing that HSCs can efficiently assimilate M2 macrophage-derived exosomes. In addition, the LX2 cells were treated with $M2^{exo}$, PBS, or WASH (PBS after washing exosomes twice) for 36 h. RT-qPCR assays showed that 50 μg/mL $M2^{exo}$ can inhibit HSCs activation as indicated by the decreased expression of *αSMA*, *COL3A1*, and *COL1A1* as compared with PBS or WASH controls (Figure 3B). Besides, the expression of *αSMA*, *COL3A1*, and *COL1A1* was significantly decreased by $M2^{exo}$ rather than PBS in TGFβ1-treated LX2 cells (Figure 3C). Western blotting results also demonstrated that M2 macrophage-derived exosomes exerted an inhibitory effect on the activation of HSCs (Figures 3D and 3E). In addition, immunofluorescence staining revealed that the expression of αSMA in TGFβ1-null or TGFβ1-activated LX2 cells was both significantly decreased by M2 macrophage-derived exosomes (Figures 3F and 3G). Taken together, our findings suggest that M2 macrophages-derived exosomes effectively inhibit the activation of HSCs.

M2 macrophage-derived exosomes inhibit HSCs activation via miR-411-5p

We further explored which component is responsible for the inhibitory effect of the exosomes on HSCs. Accordingly, we assessed the miRNA expression profiles of the exosomes derived from the serum of NASH patients or healthy controls by RNA sequencing. The subsequent analysis of the RNA-seq data revealed that 45 miRNAs were downregulated in the serum-derived exosomes of NASH patients as compared with those of healthy controls (Figure 4A). We also identified four miRNAs (miR-411-5p, miR-127-3p, miR-381-3p, and miR-541-5p) that were consistently downregulated in the NAFLD/NASH liver samples in three datasets retrieved from the Gene Expression Omnibus (GEO) database (GSE65978 (Xiao et al., 2016), GSE94799 (Guo et al., 2018), and GSE144721 (Hong et al., 2020), Figure 4B). Remarkably, only miR-411-5p among the four identified miRNAs was found to be downregulated both in serum exosomes of NASH patients and in NAFLD/NASH liver samples. We further observed that the expression of miR-411-5p was significantly decreased in the liver of rats subjected to HFHCD feeding, which was consistent with the expression of M2 macrophage markers (Figures 4C, S1A, and S1B). Moreover, we differentiated THP-1 cells into M1 macrophages using LPS and IFNγ (Figures S2A and S2B) and successfully isolated and identified their secreted exosomes (Figures S2C–S2E). As compared with the exosomes secreted by M0 macrophages or M1 macrophages, the exosomes secreted by M2 macrophages contained much higher levels of miR-411-5p (Figures 4D and 4E). Similarly, the expression of miR-411-5p was significantly higher in M2 macrophages compared to M1 macrophages (Figure S2F). These findings suggest that M2 macrophage-derived exosomes might inhibit the activation of HSCs via miR-411-5p.

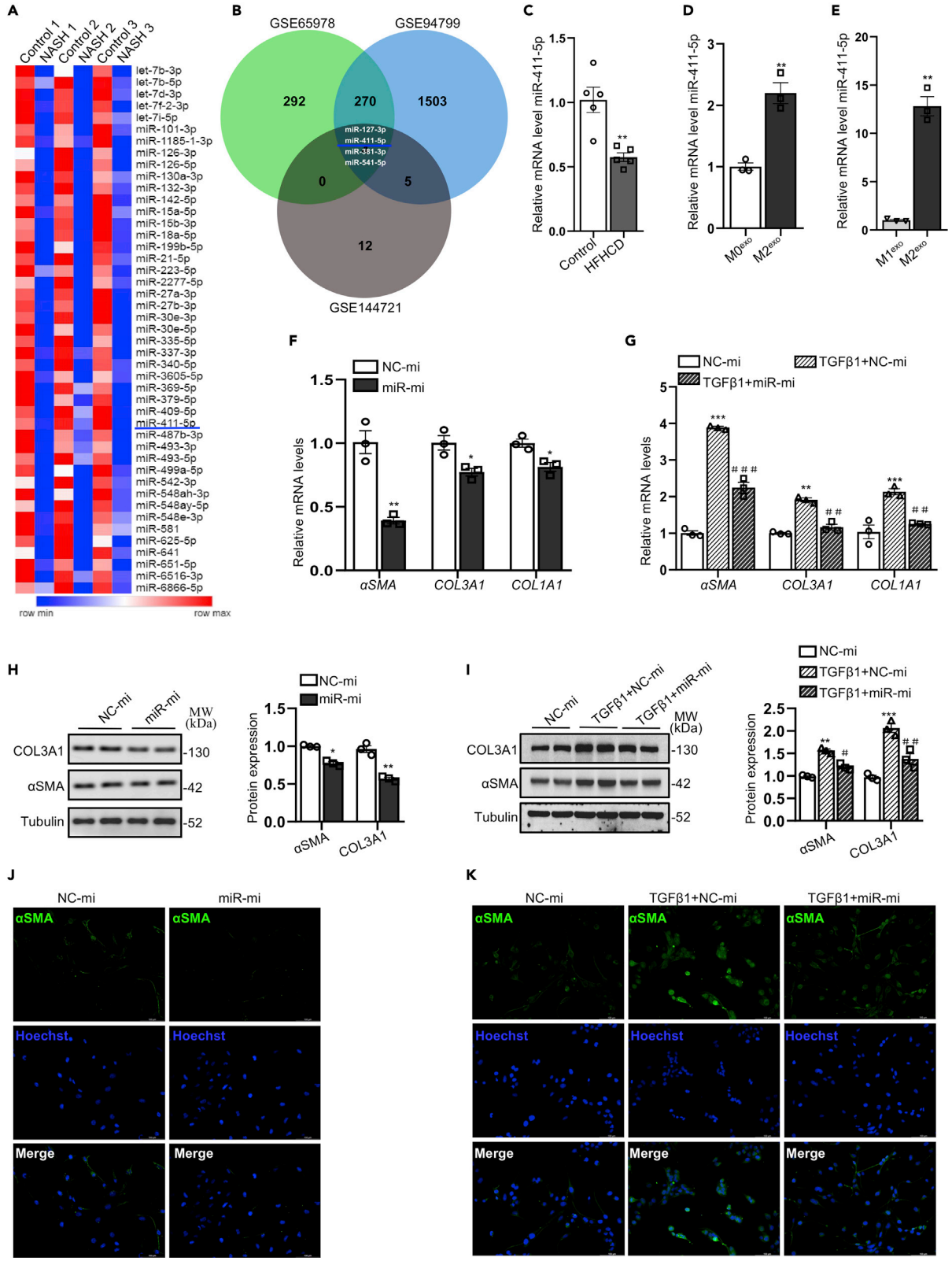
A
Control 1
NASH 1
Control 2
NASH 2
Control 3
NASH 3
let-7b-3p
let-7b-5p
let-7d-3p
let-7f-2-3p
let-7i-5p
miR-101-3p
miR-1185-1-3p
miR-126-3p
miR-126-5p
miR-130a-3p
miR-132-3p
miR-142-5p
miR-15a-5p
miR-15b-3p
miR-18a-5p
miR-199b-5p
miR-21-5p
miR-223-5p
miR-2277-5p
miR-27a-3p
miR-27b-3p
miR-30e-3p
miR-30e-5p
miR-335-5p
miR-337-3p
miR-340-5p
miR-3605-5p
miR-369-5p
miR-379-5p
miR-409-5p
miR-411-5p
miR-487b-3p
miR-493-3p
miR-493-5p
miR-499a-5p
miR-542-3p
miR-548ah-3p
miR-548ay-5p
miR-548e-3p
miR-581
miR-625-5p
miR-641
miR-651-5p
miR-6516-3p
miR-6866-5p
row min
row max
B
GSE65978
GSE94799
GSE144721
292
270
1503
miR-127-3p
miR-411-5p
miR-381-3p
miR-541-5p
0
5
12
C
Relative mRNA level miR-411-5p
Control
HFHCD
D
Relative mRNA level miR-411-5p
M0exo
M2exo
E
Relative mRNA level miR-411-5p
M1exo
M2exo
F
NC-mi
miR-mi
Relative mRNA levels
αSMA
COL3A1
COL1A1
G
NC-mi
TGFβ1+NC-mi
TGFβ1+miR-mi
Relative mRNA levels
αSMA
COL3A1
COL1A1
H
NC-mi
miR-mi
MW (kDa)
COL3A1
αSMA
Tubulin
-130
-42
-52
NC-mi
miR-mi
Protein expression
αSMA
COL3A1
I
NC-mi
TGFβ1+NC-mi
TGFβ1+miR-mi
MW (kDa)
COL3A1
αSMA
Tubulin
-130
-42
-52
NC-mi
TGFβ1+NC-mi
TGFβ1+miR-mi
Protein expression
αSMA
COL3A1
J
NC-mi
miR-mi
αSMA
Hoechst
Merge
K
NC-mi
TGFβ1+NC-mi
TGFβ1+miR-mi
αSMA
Hoechst
Merge

Figure 4. M2 macrophage-derived exosomes inhibit HSCs activation via miR-411-5p

(A) The heatmap shows the miRNA expression profiles in the exosomes isolated from serum samples of NASH patients (n = 3) or healthy controls (n = 3).
(B) The overlapping area of the Venn diagram indicating four downregulated miRNAs in the three GEO datasets.
(C) The expression of miR-411-5p in rat livers was analyzed by RT-qPCR (n = 5).
(D) Expression of miR-411-5p in the exosomes secreted by M0 and M2 macrophages was analyzed by RT-qPCR (n = 3).
(E) Expression of miR-411-5p in the exosomes secreted by M1 and M2 macrophages was analyzed by RT-qPCR (n = 3).
(F) Levels of *αSMA*, *COL1A1*, and *COL3A1* mRNA were analyzed by RT-qPCR in LX2 cells treated with 20 nM miR-411-5p mimics or NC mimics (n = 3).
(G) Levels of *αSMA*, *COL3A1*, and *COL1A1* mRNA were analyzed by RT-qPCR in TGFβ1-treated LX2 cells with miR-411-5p mimics or NC mimics (n = 3).
(H) Levels of αSMA and COL3A1 protein were analyzed by western blotting analysis in LX2 cells treated with 20 nM miR-411-5p mimics or NC mimics (n = 3).
(I) Levels of αSMA and COL3A1 protein were analyzed by western blotting analysis in TGFβ1-treated LX2 cells with miR-411-5p mimics or NC mimics (n = 3).
(J) Expression of αSMA was analyzed by immunofluorescence staining in LX2 cells treated with 20 nM miR-411-5p mimics or NC mimics (scale bar = 100μm).
(K) Expression of αSMA was analyzed by immunofluorescence staining in TGFβ1-treated LX2 cells with miR-411-5p mimics or NC mimics (scale bar = 100μm).
Data are expressed as mean ± SEM The statistical significance of the difference between the compared groups was analyzed by Student's *t*-test. *, **, and *** denote p values less than 0.05, 0.01, and 0.001, respectively, in comparison to Control, $M0^{exo}$, $M1^{exo}$ or NC-mi groups, whereas $^{\#}$, $^{\#\#}$, and $^{\#\#\#}$ represent p values less than 0.05, 0.01, and 0.001, respectively, in comparison to TGFβ1+NC-mi groups. NC-mi: NC mimics; miR-mi: miR-411-5p mimics. See also Figures S1 and S2.

We thus speculated that miR-411-5p plays an important role in inhibiting the activation of HSCs during NASH progression. To verify it, we transfected miR-411-5p mimics into LX2 cells and examined the expression of genes associated with the activation of HSCs. With successful transfection of miR-411-5p mimics suggested by a sharp increase in the levels of miR-411-5p in the LX2 cells (Figure S2G), significant inhibition of *αSMA*, *COL3A1*, and *COL1A1* transcripts in LX2 cells was observed (Figure 4F). Besides, the expression of *αSMA*, *COL3A1*, and *COL1A1* was significantly decreased in TGFβ1-treated LX2 cells with miR-411-5p mimics compared to NC mimics (Figure 4G). The protein level of αSMA in TGFβ1-null LX2 cells or TGFβ1-treated LX2 cells was also significantly decreased after treatment with miR-411-5p mimics rather than with NC mimics by western blotting and immunofluorescence assays (Figures 4H–4K). Collectively, these data illustrate that miR-411-5p plays a vital role in mediating the inhibitory effect of M2 macrophage-derived exosomes on HSCs activation.

CAMSAP1 is a direct target of miR-411-5p

To explore the molecular mechanisms underlying how miR-411-5p inactivates HSCs, we tried to identify the potential target genes of miR-411-5p. We used four miRNA-target prediction databases including miRWalk, TargetMiner, TargetScan, and miRDB to predict a set of target genes regulated by miR-411-5p. Analysis of the target prediction results identified seven genes that are more likely to be the downstream target genes of miR-411-5p as shown in the Venn diagram (Figure 5A). Furthermore, upregulating the expression of miR-411-5p using specific mimics resulted in significant downregulation of *CAMSAP1* and *PUM1* transcripts in LX2 cells, whereas the expressions of other five potential target genes (*ERBB4*, *FNIP1*, *LRP12*, *RAB3C*, *and SEMA3A*) remained unchanged (Figure 5B). Besides, the sequence alignment analysis revealed that miR-411-5p has a binding site on the 3′ untranslated region (3′UTR) of *CAMSAP1* or *PUM1* transcripts (Figure 5C). To verify the potential role of miR-411-5p in regulating *CAMSAP1* or *PUM1*, we constructed luciferase reporter plasmids containing either wild-type or mutant 3′UTRs of *CAMSAP1 or PUM1* transcripts. The results of dual-luciferase reporter assays showed that over-expression of miR-411-5p effectively reduced the luciferase activity of the wild-type *CAMSAP1* 3′UTR but not the mutant *CAMSAP1* 3′UTR (Figure 5D). On the other hand, miR-411-5p mimic did not affect the luciferase activity of wild-type *PUM1* 3′UTR (Figure 5E). Overall, these findings suggest that *CAMSAP1* is a direct target of miR-411-5p and miR-411-5p inhibits *CAMSAP1*.

Knockdown of *CAMSAP1* inhibits HSCs activation

Therefore, we speculated that knockdown of *CAMSAP1* could also inhibit HSCs activation. To confirm this hypothesis, we silenced the expression of *CAMSAP1* in LX2 cells using specific small interfering RNA (siRNA), indicated by the decreased expression of *CAMSAP1* by 70% (Figure 6A). We then found that the expression of *αSMA*, *COL1A1*, and *COL3A1* transcripts was significantly downregulated in TGFβ1-treated LX2 cells when *CAMSAP1* was silenced by siRNA (Figure 6B). Western blotting results also demonstrated that knockdown of *CAMSAP1* effectively inhibited the expression of αSMA, COL1A1, and COL3A1 (Figure 6C). In addition, the αSMA expression was evidently decreased in TGFβ1-treated LX2 cells subjected to *CAMSAP1* knockdown by immunofluorescence-based analysis (Figure 6D). Taken together, our findings have shown that knockdown of *CAMSAP1* inhibits the HSCs activation.

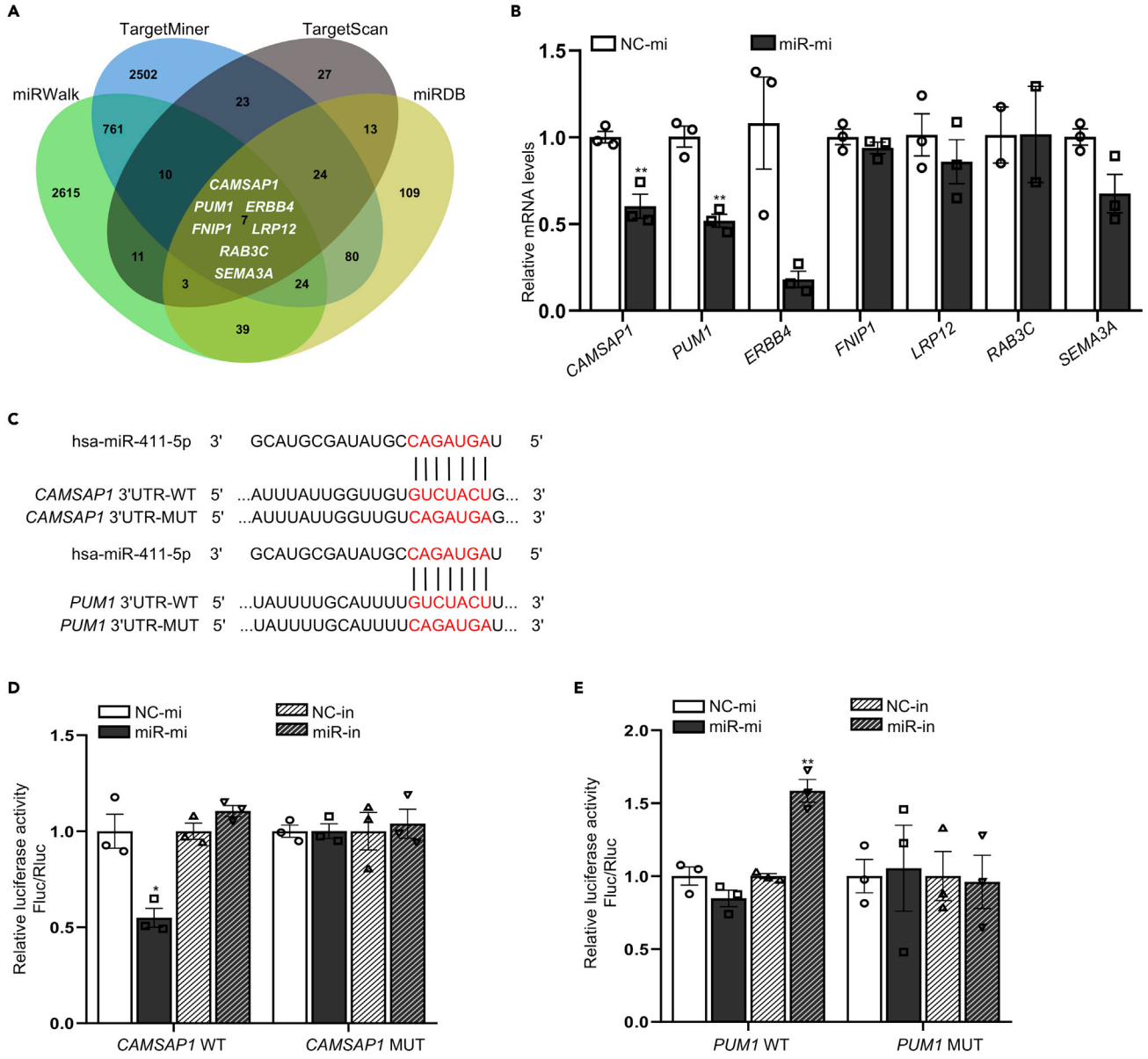

Figure 5. CAMSAP1 is a direct target of miR-411-5p

(A) Four miRNA-target gene prediction databases including miRWalk, TargetMiner, TargetScan, and miRDB were used to identify potential miR-411-5p targets.

(B) The mRNA expression of seven potential predicted targets of miR-411-5p was analyzed by RT-qPCR in LX2 cells treated with 20 nM miR-411-5p mimics or NC mimics (n = 3).

(C) The binding of *CAMSAP1* or *PUM1* 3′UTRs with miR-411-5p.

(D) Luciferase reporter assays were performed in HEK293T cells co-transfected with wild-type or mutant *CAMSAP1* 3′ UTR and miR-411-5p mimics or inhibitors (n = 3).

(E) Luciferase reporter assays in HEK293T cells co-transfected with wild-type or mutant *PUM1* 3′UTR and miR-411-5p mimics or inhibitors (n = 3). Data are expressed as mean ± SEM The statistical significance of the difference between the compared groups was analyzed by Student's *t*-test. *, and ** denote p values less than 0.05, and 0.01, respectively, in comparison to NC-mi or NC-in groups. NC-mi: NC mimics; miR-mi: miR-411-5p mimics; NC-in: NC inhibitor; miR-in: miR-411-5p inhibitor.

DISCUSSION

Although the molecular mechanisms underlying the progression from NAFL to NASH are still unclear, a few of studies have shown that HSCs and their interaction with macrophages are crucial to the HSCs activation

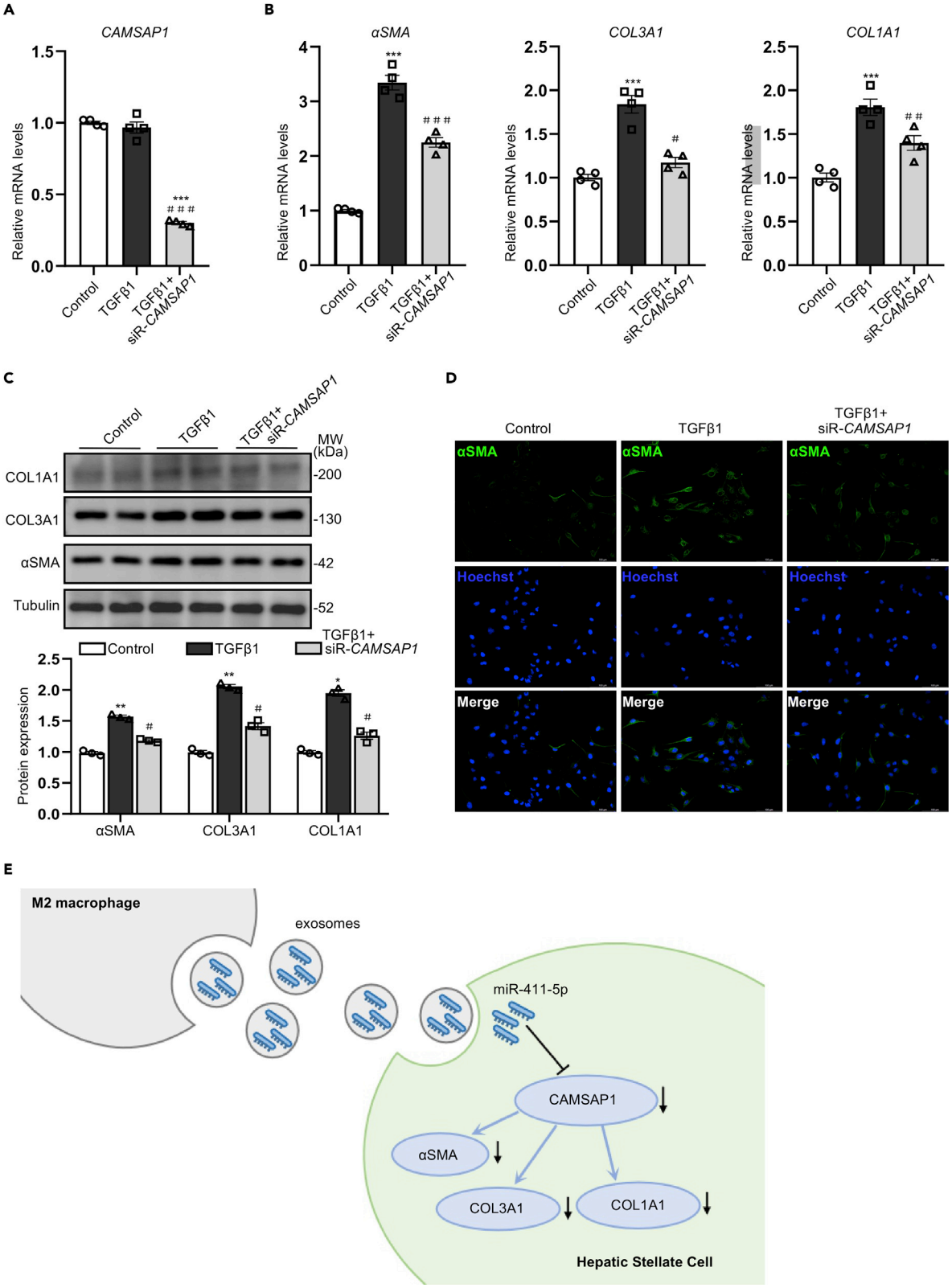
A
CAMSAP1
Relative mRNA levels
Control
TGFβ1
TGFβ1+ siR-CAMSAP1
B
αSMA
COL3A1
COL1A1
C
MW (kDa)
COL1A1
COL3A1
αSMA
Tubulin
-200
-130
-42
-52
Protein expression
D
αSMA
Hoechst
Merge
E
M2 macrophage
exosomes
miR-411-5p
CAMSAP1
αSMA
COL3A1
COL1A1
Hepatic Stellate Cell

Figure 6. Knockdown of CAMSAP1 inhibits hepatic stellate cell activation

(A) Levels of *CAMSAP1* mRNA was analyzed by RT-qPCR in TGFβ1-treated LX2 cells subjected to *CAMSAP1* knockdown with 100 nM *CAMSAP1* siRNA or Control siRNA (n = 4).

(B) Levels of *αSMA*, *COL1A1*, and *COL3A1* mRNA were analyzed by RT-qPCR in TGFβ1-treated LX2 cells subjected to *CAMSAP1* knockdown with 100nM *CAMSAP1* siRNA or Control siRNA (n = 4).

(C) Levels of αSMA, COL1A1, and COL3A1 protein were analyzed by western blotting analysis in TGFβ1-treated LX2 cells subjected to *CAMSAP1* knockdown with 100nM *CAMSAP1* siRNA or Control siRNA (n = 3).

(D) Expression of αSMA was analyzed by immunofluorescence staining in TGFβ1-treated LX2 cells subjected to *CAMSAP1* knockdown with 100nM *CAMSAP1* siRNA or Control siRNA (scale bar = 100μm).

(E) A schematic diagram showing that M2 macrophage-derived exosomes inhibit the activation of HSCs and this inhibition is mediated by miR-411-5p. MiR-411-5p can directly down-regulate the expression of *CAMSAP1* to inactivate stellate cells, and knockdown of *CAMSAP1* also inhibits the activation of HSCs. Data are expressed as mean ± SEM The statistical significance of the difference between the compared groups was analyzed by one-way ANOVA. *, **, and *** denote p values less than 0.05, 0.01, and 0.001, respectively, in comparison to Control groups; $^{\#}$, $^{\#\#}$, and $^{\#\#\#}$ denote p values less than 0.05, 0.01, and 0.001, respectively, in comparison to TGFβ1+Control siRNA groups. siR-*CAMSAP1*: *CAMSAP1* siRNA.

and progression of NASH (Harley et al., 2014; Miura et al., 2010). In the current study, we have found that in the HFHCD-induced rat model of NASH, mild fibrosis is manifested in the liver, whereas the expression of M2 macrophage markers was significantly decreased as compared to that in normal control diet-fed rats. In addition, the expression of miR-411-5p was decreased both in the liver of NASH rats and in serum exosomes of NASH patients. We further proved that M2 macrophage-derived exosomes can significantly inhibit HSCs activation and this inhibition is implemented in part, by miR-411-5p. Notably, miR-411-5p directly downregulates the expression of *CAMSAP1*, whereas silencing the expression of *CAMSAP1* also inhibits HSCs activation (Figure 6E).

Because it is difficult to fully develop severe steatohepatitis and advanced fibrosis by diet-based models (Guo et al., 2017; Liu et al., 2021), we therefore focused on the stages of NASH with mild fibrosis after feeding the rats with HFHCD for 16 weeks. This is consistent with the previous opinions that diet-based models are hard to develop advanced fibrosis (Asgharpour et al., 2016; Tsuchida et al., 2018) In the NASH progression, quiescent HSCs are transformed into activated HSCs (Devaraj et al., 2021; Zisser et al., 2021). Hepatic macrophages are involved in the activation of HSCs. For instance, hepatic macrophages can activate HSCs by releasing TNFα or IL17 (Seki and Schwabe, 2015) and TGFβ1 (Dooley and ten Dijke, 2012). Furthermore, IL22 can not only directly inhibit HSCs proliferation but also inhibit their activation by increasing the M2/M1-Kupffer cells ratio (Hu et al., 2016; Su et al., 2021). However, the crosstalk between macrophages and HSCs can also be achieved through exosomes. Lipopolysaccharide-stimulated macrophages promote HSCs activation by secreting exosomes (Chen et al., 2020). Our study has demonstrated that M2 macrophages can inhibit HSCs activation through the released exosomes and uncovered the crosstalk between M2 macrophages and HSCs is mediated by exosomes.

Exosomes can prevent the destruction of biologically active substances and transfer them to recipient cells for their biological functions (Kim et al., 2015; Raposo and Stoorvogel, 2013). The shuttling of miRNAs mediated by exosomes is an important way of intercellular communication that also affects the progression of NAFLD/NASH (Hou et al., 2021; Liu et al., 2020; Luo et al., 2021). Exosomal miR-223 from IL6-activated macrophages has been documented to contribute to the alleviation of NAFLD-related fibrosis (Hou et al., 2021). Furthermore, exosomes secreted from lipotoxic hepatocytes have been shown to contribute to the miR-192-5p-mediated activation of M1 macrophages in NAFLD (Liu et al., 2020). In our study, we determined the downregulation of miR-411-5p in serum exosomes of NASH patients and NAFLD/NASH liver samples. In the NASH model, the expression of miR-411-5p is consistent with the expression of M2 macrophage markers, wherein both are found to be significantly decreased. Moreover, the content of miR-411-5p in exosomes secreted by M2 macrophages is higher than that in M1 macrophages. MiR-411-5p is involved in the regulation of hepatocellular carcinoma progression (Chen et al., 2021b; Liu et al., 2018); however, there are no reports as yet about the regulatory function of miR-411-5p in HSCs, especially in relevance to NASH. Remarkably, our results have evidently demonstrated that miR-411-5p can effectively inhibit HSCs activation.

To further explore the potential mechanisms underlying the role of miR-411-5p in the regulation of HSCs, we sought to identify the downstream target genes that might be regulated by miR-411-5p. Through the prediction of target genes using four databases, sequence alignment studies, and dual-luciferase reporter assays, we evidently determined *CAMSAP1* as a direct target gene of miR-411-5p. Furthermore, our results demonstrated that overexpression of miR-411-5p can significantly reduce the expression of *CAMSAP1* in

HSCs. *CAMSAP1* is reportedly expressed in mammalian astrocytes and known to regulate the multipolar-bipolar transition of cortical neurons (Yamamoto et al., 2009; Zhou et al., 2020). Until now, we have not come across any study that has comprehensively investigated the role of *CAMSAP1* in liver diseases, especially NASH. Our study not only proved that *CAMSAP1* is directly targeted by miR-411-5p but also showed that knockdown of *CAMSAP1* can effectively inhibit HSCs activation.

In conclusion, we have provided solid experimental evidence demonstrating that exosomal miRNA-411-5p derived from M2 macrophages plays an inhibitory role in HSCs activation during NASH progression by inhibiting its target gene *CAMSAP1*. Our findings thus provide an insight into the vital role of exosomes in the crosstalk between the M2 macrophages and the HSCs and reveal a potential mechanism underlying the pathological progression of NASH. The findings also provide further insights to facilitate better understanding of the anti-fibrosis effect of M2 macrophages. Importantly, this study suggests a potential role of *CAMSAP1* as a promising target for NASH treatment.

Limitations of the study

However, our study has some limitations. We did not observe the expression of CAMSAP1 by western blotting because CAMSAP1 antibody is unavailable. Besides, the study did not validate the role of *CAMSAP1 in vivo*. Thus, further studies are essential to address this limitation.

STAR★METHODS

Detailed methods are provided in the online version of this paper and include the following:

- KEY RESOURCES TABLE
- RESOURCE AVAILABILITY
  - Lead contact
  - Materials availability
  - Data and code availability
- EXPERIMENTAL MODEL AND SUBJECT DETAILS
  - Human serum exosomal RNA sequencing and datasets
  - Animal studies
- METHOD DETAILS
  - Cell culture and treatment
  - Exosome isolation and identification
  - Exosome uptake assays
  - Western blotting
  - RNA extraction and quantitative reverse transcription PCR
  - Flow cytometry
  - Histopathology and immunohistochemistry studies
  - Immunofluorescence analysis
  - Dual-luciferase reporter assay
- QUANTIFICATION AND STATISTICAL ANALYSIS

SUPPLEMENTAL INFORMATION

Supplemental information can be found online at https://doi.org/10.1016/j.isci.2022.104597.

ACKNOWLEDGMENTS

We thank the members of our laboratory for their support and technical help. We would also like to acknowledge the NCBI's GEO database for providing access to datasets crucial for validating the findings of this study and their contributors for their valuable public data sets. This work was supported by the National Natural Science Foundation of China [No. 81870597, No. 81970741], the Science and Technology Program of Guangzhou [202102010229], and the Local Innovative and Research Teams Projects of Guangdong Pearl River Talents Program [2017BT 01S131].

AUTHOR CONTRIBUTIONS

Z.W., H.D., and F.X. conceived and designed the study. Z.W. and X.Y. performed most of the experiments and analyzed the data. X.L., Y.S., and P.Y. performed some of the experiments. Z.W., H.D., and F.X.

analyzed data and wrote the manuscript. All the authors have reviewed and approved the final version of the manuscript.

DECLARATION OF INTERESTS

The authors declare no competing interests.

Received: January 25, 2022
Revised: April 29, 2022
Accepted: June 7, 2022
Published: July 15, 2022

REFERENCES

Androvic, P., Valihrach, L., Elling, J., Sjoback, R., and Kubista, M. (2017). Two-tailed RT-qPCR: a novel method for highly accurate miRNA quantification. Nucleic Acids Res. *45*, e144. https://doi.org/10.1093/nar/gkx588.

Asgharpour, A., Cazanave, S.C., Pacana, T., Seneshaw, M., Vincent, R., Banini, B.A., Kumar, D.P., Daita, K., Min, H.K., Mirshahi, F., et al. (2016). A diet-induced animal model of non-alcoholic fatty liver disease and hepatocellular cancer. J. Hepatol. *65*, 579–588. https://doi.org/10.1016/j.jhep.2016.05.005.

Bartel, D.P. (2009). MicroRNAs: target recognition and regulatory functions. Cell *136*, 215–233. https://doi.org/10.1016/j.cell.2009.01.002.

Benbow, J.H., Marrero, E., McGee, R.M., Brandon-Warner, E., Attal, N., Feilen, N.A., Culberson, C.R., McKillop, I.H., and Schrum, L.W. (2021). Hepatic stellate cell-derived exosomes modulate macrophage inflammatory response. Exp. Cell Res. *405*, 112663. https://doi.org/10.1016/j.yexcr.2021.112663.

Chanput, W., Mes, J.J., and Wichers, H.J. (2014). THP-1 cell line: an in vitro cell model for immune modulation approach. Int. Immunopharmacol. *23*, 37–45. https://doi.org/10.1016/j.intimp.2014.08.002.

Chen, L., Charrier, A., Zhou, Y., Chen, R., Yu, B., Agarwal, K., Tsukamoto, H., Lee, L.J., Paulaitis, M.E., and Brigstock, D.R. (2014). Epigenetic regulation of connective tissue growth factor by MicroRNA-214 delivery in exosomes from mouse or human hepatic stellate cells. Hepatology *59*, 1118–1129. https://doi.org/10.1002/hep.26768.

Chen, L., Chen, R., Velazquez, V.M., and Brigstock, D.R. (2016). Fibrogenic signaling is suppressed in hepatic stellate cells through targeting of connective tissue growth factor (CCN2) by cellular or exosomal MicroRNA-199a-5p. Am. J. Pathol. *186*, 2921–2933. https://doi.org/10.1016/j.ajpath.2016.07.011.

Chen, L., Huang, Y., Duan, Z., Huang, P., Yao, H., Zhou, Y., Ji, Q., and Liu, X. (2021a). Exosomal miR-500 derived from lipopolysaccharide-treated macrophage accelerates liver fibrosis by suppressing MFN2. Front. Cell Dev. Biol. *9*, 716209. https://doi.org/10.3389/fcell.2021.716209.

Chen, L., Yao, X., Yao, H., Ji, Q., Ding, G., and Liu, X. (2020). Exosomal miR-103-3p from LPS-activated THP-1 macrophage contributes to the activation of hepatic stellate cells. FASEB. J. *34*, 5178–5192. https://doi.org/10.1096/fj.201902307rrr.

Chen, T., Liu, R., Niu, Y., Mo, H., Wang, H., Lu, Y., Wang, L., Sun, L., Wang, Y., Tu, K., et al. (2021b). HIF-1alpha-activated long non-coding RNA KDM4A-AS1 promotes hepatocellular carcinoma progression via the miR-411-5p/KPNA2/AKT pathway. Cell Death Dis. *12*, 1152. https://doi.org/10.1038/s41419-021-04449-2.

Cheng, D., Chai, J., Wang, H., Fu, L., Peng, S., and Ni, X. (2021). Hepatic macrophages: key players in the development and progression of liver fibrosis. Liver Int. *41*, 2279–2294. https://doi.org/10.1111/liv.14940.

Devaraj, E., Perumal, E., Subramaniyan, R., and Mustapha, N. (2021). Liver fibrosis: extracellular vesicles mediated intercellular communication in perisinusoidal space. Hepatology. https://doi.org/10.1002/hep.32239.

Diehl, A.M., and Day, C. (2017). Cause, pathogenesis, and treatment of nonalcoholic steatohepatitis. N. Engl. J. Med. *377*, 2063–2072. https://doi.org/10.1056/nejmra1503519.

Dooley, S., and ten Dijke, P. (2012). TGF-beta in progression of liver disease. Cell Tissue Res. *347*, 245–256. https://doi.org/10.1007/s00441-011-1246-y.

Genin, M., Clement, F., Fattaccioli, A., Raes, M., and Michiels, C. (2015). M1 and M2 macrophages derived from THP-1 cells differentially modulate the response of cancer cells to etoposide. BMC Cancer *15*, 577. https://doi.org/10.1186/s12885-015-1546-9.

Gordon, S., and Taylor, P.R. (2005). Monocyte and macrophage heterogeneity. Nat. Rev. Immunol. *5*, 953–964. https://doi.org/10.1038/nri1733.

Guo, L., Zhang, P., Chen, Z., Xia, H., Li, S., Zhang, Y., Kobberup, S., Zou, W., and Lin, J.D. (2017). Hepatic neuregulin 4 signaling defines an endocrine checkpoint for steatosis-to-NASH progression. J. Clin. Invest. *127*, 4449–4461. https://doi.org/10.1172/jci96324.

Guo, J., Zhou, Y., Cheng, Y., Fang, W., Hu, G., Wei, J., Lin, Y., Man, Y., Guo, L., Sun, M., et al. (2018). Metformin-Induced Changes of the Coding Transcriptome and Non-Coding RNAs in the Livers of Non-Alcoholic Fatty Liver Disease Mice. Cell Physiol Biochem *45*, 1487–1505. https://doi.org/10.1159/000487575.

Harley, I.T., Stankiewicz, T.E., Giles, D.A., Softic, S., Flick, L.M., Cappelletti, M., Sheridan, R., Xanthakos, S.A., Steinbrecher, K.A., Sartor, R.B., et al. (2014). IL-17 signaling accelerates the progression of nonalcoholic fatty liver disease in mice. Hepatology *59*, 1830–1839. https://doi.org/10.1002/hep.26746.

Hong, W., Li, S., Cai, Y., Zhang, T., Yang, Q., He, B., Yu, J., and Chen, Z. (2020). The Target MicroRNAs and Potential Underlying Mechanisms of Yiqi-Bushen-Tiaozhi Recipe against-Non-Alcoholic Steatohepatitis. Front Pharmacol *11*, 529553. https://doi.org/10.3389/fphar.2020.529553.

Hou, X., Yin, S., Ren, R., Liu, S., Yong, L., Liu, Y., Li, Y., Zheng, M.H., Kunos, G., Gao, B., et al. (2021). Myeloid-cell-specific IL-6 signaling promotes MicroRNA-223-enriched exosome production to attenuate NAFLD-associated fibrosis. Hepatology *74*, 116–132. https://doi.org/10.1002/hep.31658.

Hu, B.L., Shi, C., Lei, R.E., Lu, D.H., Luo, W., Qin, S.Y., Zhou, Y., and Jiang, H.X. (2016). Interleukin-22 ameliorates liver fibrosis through miR-200a/beta-catenin. Sci. Rep. *6*, 36436. https://doi.org/10.1038/srep36436.

Huntzinger, E., and Izaurralde, E. (2011). Gene silencing by microRNAs: contributions of translational repression and mRNA decay. Nat. Rev. Genet. *12*, 99–110. https://doi.org/10.1038/nrg2936.

Kim, D.K., Lee, J., Kim, S.R., Choi, D.S., Yoon, Y.J., Kim, J.H., Go, G., Nhung, D., Hong, K., Jang, S.C., et al. (2015). EVpedia: a community web portal for extracellular vesicles research. Bioinformatics *31*, 933–939. https://doi.org/10.1093/bioinformatics/btu741.

Lane, R.E., Korbie, D., Trau, M., and Hill, M.M. (2017). Purification protocols for extracellular vesicles. Methods Mol. Biol. *1660*, 111–130. https://doi.org/10.1007/978-1-4939-7253-1_10.

Liu, B., Xiang, L., Ji, J., Liu, W., Chen, Y., Xia, M., Liu, Y., Liu, W., Zhu, P., Jin, Y., et al. (2021). Sparcl1 promotes nonalcoholic steatohepatitis progression in mice through upregulation of CCL2. J. Clin. Invest. *131*, e144801.

Liu, H., Xue, L., Song, C., Liu, F., Jiang, T., and Yang, X. (2018). Overexpression of circular RNA circ_001569 indicates poor prognosis in hepatocellular carcinoma and promotes cell growth and metastasis by sponging miR-411-5p and miR-432-5p. Biochem. Biophys. Res.

Commun. *503*, 2659–2665. https://doi.org/10.1016/j.bbrc.2018.08.020.

Liu, X.L., Pan, Q., Cao, H.X., Xin, F.Z., Zhao, Z.H., Yang, R.X., Zeng, J., Zhou, H., and Fan, J.G. (2020). Lipotoxic hepatocyte-derived exosomal MicroRNA 192-5p activates macrophages through rictor/akt/forkhead box transcription factor O1 signaling in nonalcoholic fatty liver disease. Hepatology *72*, 454–469. https://doi.org/10.1002/hep.31050.

Luo, X., Luo, S.Z., Xu, Z.X., Zhou, C., Li, Z.H., Zhou, X.Y., and Xu, M.Y. (2021). Lipotoxic hepatocyte-derived exosomal miR-1297 promotes hepatic stellate cell activation through the PTEN signaling pathway in metabolic-associated fatty liver disease. World J. Gastroenterol. *27*, 1419–1434. https://doi.org/10.3748/wjg.v27.i14.1419.

Miura, K., Kodama, Y., Inokuchi, S., Schnabl, B., Aoyama, T., Ohnishi, H., Olefsky, J.M., Brenner, D.A., and Seki, E. (2010). Toll-like receptor 9 promotes steatohepatitis by induction of interleukin-1β in mice. Gastroenterology *139*, 323–334.e7. https://doi.org/10.1053/j.gastro.2010.03.052.

Potrich, C., Lunelli, L., Vaghi, V., Pasquardini, L., and Pederzolli, C. (2017). Cell transfer of information via miR-loaded exosomes: a biophysical approach. Eur. Biophys. J. *46*, 803–811. https://doi.org/10.1007/s00249-017-1262-2.

Raposo, G., and Stoorvogel, W. (2013). Extracellular vesicles: exosomes, microvesicles, and friends. J. Cell Biol. *200*, 373–383. https://doi.org/10.1083/jcb.201211138.

Sakai, Y., Chen, G., Ni, Y., Zhuge, F., Xu, L., Nagata, N., Kaneko, S., Ota, T., and Nagashimada, M. (2020). DPP-4 inhibition with anagliptin reduces lipotoxicity-induced insulin resistance and steatohepatitis in male mice. Endocrinology *161*, bqaa139. https://doi.org/10.1210/endocr/bqaa139.

Seki, E., and Schwabe, R.F. (2015). Hepatic inflammation and fibrosis: functional links and key pathways. Hepatology *61*, 1066–1079. https://doi.org/10.1002/hep.27332.

Sheka, A.C., Adeyi, O., Thompson, J., Hameed, B., Crawford, P.A., and Ikramuddin, S. (2020). Nonalcoholic steatohepatitis: a review. JAMA *323*, 1175–1183. https://doi.org/10.1001/jama.2020.2298.

Su, S.B., Qin, S.Y., Xian, X.L., Huang, F.F., Huang, Q.L., ZhangDi, H.J., and Jiang, H.X. (2021). Interleukin-22 regulating Kupffer cell polarization through STAT3/Erk/Akt crosstalk pathways to extenuate liver fibrosis. Life Sci. *264*, 118677. https://doi.org/10.1016/j.lfs.2020.118677.

Tacke, F., and Zimmermann, H.W. (2014). Macrophage heterogeneity in liver injury and fibrosis. J. Hepatol. *60*, 1090–1096. https://doi.org/10.1016/j.jhep.2013.12.025.

Théry, C., Witwer, K.W., Aikawa, E., Alcaraz, M.J., Anderson, J.D., Andriantsitohaina, R., Antoniou, A., Arab, T., Archer, F., Atkin-Smith, G.K., et al. (2018). Minimal information for studies of extracellular vesicles 2018 (MISEV2018): a position statement of the International Society for Extracellular Vesicles and update of the MISEV2014 guidelines. J. Extracell. Vesicles *7*, 1535750. https://doi.org/10.1080/20013078.2018.1535750.

Tsuchida, T., Lee, Y.A., Fujiwara, N., Ybanez, M., Allen, B., Martins, S., Fiel, M.I., Goossens, N., Chou, H.I., Hoshida, Y., et al. (2018). A simple diet- and chemical-induced murine NASH model with rapid progression of steatohepatitis, fibrosis and liver cancer. J. Hepatol. *69*, 385–395. https://doi.org/10.1016/j.jhep.2018.03.011.

Wan, J., Benkdane, M., Teixeira-Clerc, F., Bonnafous, S., Louvet, A., Lafdil, F., Pecker, F., Tran, A., Gual, P., Mallat, A., et al. (2014). M2 Kupffer cells promote M1 Kupffer cell apoptosis: a protective mechanism against alcoholic and nonalcoholic fatty liver disease. Hepatology *59*, 130–142. https://doi.org/10.1002/hep.26607.

Wang, L., Wang, Y., and Quan, J. (2020). Exosomal miR-223 derived from natural killer cells inhibits hepatic stellate cell activation by suppressing autophagy. Mol. Med. *26*, 81. https://doi.org/10.1186/s10020-020-00207-w.

Xiao, J., Bei, Y., Liu, J., Dimitrova-Shumkovska, J., Kuang, D., Zhou, Q., Li, J., Yang, Y., Xiang, Y., Wang, F., et al. (2016). miR-212 downregulation contributes to the protective effect of exercise against non-alcoholic fatty liver via targeting FGF-21. J Cell Mol Med *20*, 204–216. https://doi.org/10.1111/jcmm.12733.

Yamamoto, M., Yoshimura, K., Kitada, M., Nakahara, J., Seiwa, C., Ueki, T., Shimoda, Y., Ishige, A., Watanabe, K., and Asou, H. (2009). A new monoclonal antibody, A3B10, specific for astrocyte-lineage cells recognizes calmodulin-regulated spectrin-associated protein 1 (Camsap1). J. Neurosci. Res. *87*, 503–513. https://doi.org/10.1002/jnr.21853.

Yanez-Mo, M., Siljander, P.R.M., Andreu, Z., Bedina Zavec, A., Borràs, F.E., Buzas, E.I., Buzas, K., Casal, E., Cappello, F., Carvalho, J., et al. (2015). Biological properties of extracellular vesicles and their physiological functions. J. Extracell. Vesicles *4*, 27066. https://doi.org/10.3402/jev.v4.27066.

Yang, Y., Wu, X.Q., Li, W.X., Huang, H.M., Li, H.D., Pan, X.Y., Li, X.F., Huang, C., Meng, X.M., Zhang, L., et al. (2018). PSTPIP2 connects DNA methylation to macrophage polarization in CCL4-induced mouse model of hepatic fibrosis. Oncogene *37*, 6119–6135. https://doi.org/10.1038/s41388-018-0383-0.

Younossi, Z., Tacke, F., Arrese, M., Chander Sharma, B., Mostafa, I., Bugianesi, E., Wai-Sun Wong, V., Yilmaz, Y., George, J., Fan, J., et al. (2019). Global perspectives on nonalcoholic fatty liver disease and nonalcoholic steatohepatitis. Hepatology *69*, 2672–2682. https://doi.org/10.1002/hep.30251.

Zhou, Z., Xu, H., Li, Y., Yang, M., Zhang, R., Shiraishi, A., Kiyonari, H., Liang, X., Huang, X., Wang, Y., et al. (2020). CAMSAP1 breaks the homeostatic microtubule network to instruct neuronal polarity. Proc. Natl. Acad. Sci. U S A *117*, 22193–22203. https://doi.org/10.1073/pnas.1913177117.

Zisser, A., Ipsen, D.H., and Tveden-Nyborg, P. (2021). Hepatic stellate cell activation and inactivation in NASH-fibrosis-roles as putative treatment targets? Biomedicines *9*, 365. https://doi.org/10.3390/biomedicines9040365.

STAR★METHODS

KEY RESOURCES TABLE

REAGENT or RESOURCE	SOURCE	IDENTIFIER
Antibodies		
Goat Anti-Rabbit IgG H&L (HRP)	Abcam	Cat# ab6721; RRID: AB_955447
Rabbit anti-αSMA	Abcam	Cat# ab32575; RRID: AB_722538
Rabbit anti-COL1A1	Abcam	Cat# ab138492; RRID: AB_2861258
Rabbit anti-COL3A1	Abcam	Cat# ab184993; RRID: AB_2895112
Rabbit anti-Tubulin	Cell Signaling Technology	Cat# 2128; RRID: AB_823664
Rabbit anti-CD163	Servicebio	Cat# GB13340; RRID: AB_2892095
Mouse anti-CD86-PE	eBioscience	Cat# 12-0869-42; RRID: AB_10732345
Mouse anti-CD206-APC	eBioscience	Cat# 17-2069-42; RRID: AB_2573182
Biological samples		
Human blood	The Third Affiliated Hospital, Sun Yat-sen University	N/A
Chemicals, peptides, and recombinant proteins		
Dulbecco's modified Eagle's medium	Gibco	Cat# C11995500BT
RPMI-1640	Gibco	Cat# C11875500BT
Fetal Bovine Serum	Gibco	Cat# 10270-106
PMA	Sigma-Aldrich	Cat# P8139
LPS	Sigma-Aldrich	Cat# L4391-1MG
IFNγ	PeproTech	Cat# 96-300-02-20
IL4	PeproTech	Cat# 200-04-5
IL13	PeproTech	Cat# 200-13-2
TGFβ1	PeproTech	Cat# 100-21-10
miRNA mimic/NC	Ribo	Cat# miR1020
CAMSAP1 siRNA	Ribo	Cat# siBDM2500-15
Hoechst dye	Phygene	Cat# PH0528
Radio-immunoprecipitation assay (RIPA) buffer	ThermoFisher	Cat# 89900
TRIzol	Invitrogen	Cat# 15596018
TB Green Premix Ex TaqII	Takara	Cat# RR820A
Haematoxylin and Eosin dye	Servicebio	Cat# G1003
Masson dye	Servicebio	Cat# G1006
Oil Red O dye	Servicebio	Cat# G1016
DAB	Servicebio	Cat# G1211
Triton-X-100	Sigma-Aldrich	Cat# T9284
BSA	Servicebio	Cat# G1211
Critical commercial assays		
MINI26-1KT PKH26	Sigma-Aldrich	Cat# MINI26-1KT
Deposited data		
miRNA expression profiles (Raw and analyzed data)	This paper	GEO: GSE202167
Experimental models: Cell lines		
Human monocyte cell line THP-1	Chinese Academy of Sciences Cell Bank	Cat# TCHu 57

(*Continued on next page*)

Continued

REAGENT or RESOURCE	SOURCE	IDENTIFIER
Human hepatic stellate cell line LX2	CellCook	Cat# CC4023
Experimental models: Organisms/strains		
Sprague Dawley Rats	Guangzhou University of Chinese Medicine	N/A
Oligonucleotides		
RT-qPCR primers, see Table S1	This paper	N/A
Software and algorithms		
FlowJo 10.0	Treestar	https://www.flowjo.com/solutions/flowjo
Leica software package	Leica	N/A
ImageJ software	NIH	https://imagej.nih.gov/ij/
GraphPad Prism 8.0	GraphPad Software	https://www.graphpad.com/
CytExpert software 2.3	Beckman Coulter	N/A
Other		
High-fat high-cholesterol diet	ReadyDietech	Cat# D10070802
Regular chow diet	ReadyDietech	Cat# RDCX-1

RESOURCE AVAILABILITY

Lead contact

Further information and requests for resources and reagents should be directed to and will be fulfilled by the lead contact, Hong Deng (dhong@mail.sysu.edu.cn).

Materials availability

This study did not generate new unique reagents.

Data and code availability

- All data reported in this paper will be shared by the lead contact upon request.
- This paper does not report original code.
- Any additional information required to reanalyze the data reported in this paper is available from the lead contact upon request.

EXPERIMENTAL MODEL AND SUBJECT DETAILS

Human serum exosomal RNA sequencing and datasets

The study involving human subjects was approved by the Medical Ethics Committee of the Third Affiliated Hospital of Sun Yat-sen University, Guangzhou, P. R. China. The NAFLD patients were recruited from the infectious disease outpatient clinic at the Third Affiliated Hospital of Sun Yat-sen University; healthy controls were recruited from hospital staff and graduate. Informed consents were obtained from all the NAFLD patients and healthy controls included in the study. Blood samples were collected from healthy controls (n = 3) and patients with biopsy-proven NASH (n = 3). The mean age of the patients was 32 years old. 3 patients were male and 3 were female. Exosomal miRNAs were sequenced by Guangzhou RiboBio (Guangzhou, P. R. China) using an Illumina HiSeq 2500 platform. Additionally, the miRNA expression profiles of control liver and NAFLD/NASH liver tissues were obtained from the three datasets namely, GSE65978, GSE94799, and GSE144721, available at Gene Expression Omnibus database (www.ncbi.nlm.nih.gov/geo).

Animal studies

The animal experiments were approved by the ethics committee and complied with the ARRIVE guidelines as well as the National Institute of Health's Guide for the Care and Use of Laboratory Animals. Male Sprague-Dawley (SD) rats (aged seven weeks) were purchased from Guangzhou University of Chinese

Medicine (Guangzhou, P. R. China) and housed in a temperature-controlled pathogen-free environment on a 12 hours light/dark cycle, with *ad libitum* access to food and water. After a one-week acclimatization period, these SD rats were randomly assigned to two groups: fed *ad libitum* with a regular chow or a high-fat high-cholesterol diet (HFHCD, 88% standard diet, 10% lard, and 2% cholesterol) (Readydietech, China), for 16 weeks. Finally, five rats in each group were starved overnight; their blood samples and livers were collected after euthanasia and were stored at −80°C.

METHOD DETAILS

Cell culture and treatment

The human liver stellate cells (LX2) and the human acute monocytic leukaemia cells (THP-1) were cultured in high-glucose Dulbecco's modified Eagle's medium (Cat# C11995500BT, Gibco, Thermo Fisher Scientific Corp., MA, USA) and RPMI-1640 (Cat# C11875500BT, Gibco, Thermo Fisher Scientific Corp., MA, USA), respectively in the presence of 10% fetal bovine serum (FBS; Cat# 10270-106; Gibco, Thermo Fisher Scientific Corp., MA, USA). The cells were incubated in a humidified incubation chamber (Thermo Fisher Scientific Corp., MA, USA) at 37°C with 5% CO_2. Macrophage M1 polarization and Macrophage M2 polarization were performed as reported previously(Chanput et al., 2014; Genin et al., 2015). Briefly, the THP-1 monocytes were treated with 100 ng/mL PMA (Cat# P8139, Sigma-Aldrich, MO, USA) for 24 hours to induce differentiation into macrophages, and the macrophage M1 polarization was attained post incubation with 100 ng/mL of lipopolysaccharide (LPS; Cat# L4391-1MG; Sigma-Aldrich, MO, USA) and 20 ng/mL of IFNγ (Cat# 96-300-02-20; PeproTech, NJ, USA) for 48 hours, or the macrophage M2 polarization was attained post incubation with 20 ng/mL of interleukin 4 (IL4; Cat# 200-04-5; PeproTech, NJ, USA) and 20 ng/mL of interleukin 13 (IL13; Cat# 200-13-2; PeproTech, NJ, USA) for 48 hours. Prior to the treatment of cells with 20 nM of miRNA mimic (Cat# miR1020, Ribo, Guangzhou, P. R. China), 100 nM of *CAMSAP1* siRNA (Cat# siBDM2500-15, Ribo, Guangzhou, P. R. China), and 10 ng/mL of TGFβ1 (Cat# 100-21-10, PeproTech, NJ, USA), the cells were cultured in serum-free medium overnight.

Exosome isolation and identification

Exosomes were collected from the M2 macrophage culture spent medium by ultrafiltration as reported previously (Lane et al., 2017; Théry et al., 2018). Briefly, the cultured supernatants were collected, and the exosomes were purified by sequential centrifugation at 600 × g for 10 min, followed by 2000 × g for 30 min at 4°C to remove the cells and cellular debris. Next, the supernatants were filtered through a 0·22 μm filter membrane (Cat# SLGP033RB, Millipore, MA, USA) to remove large vesicles. The supernatants mainly containing the exosomes were further concentrated to 150 μL by Amicon ultra-15 centrifugal filter (Cat# UFC910096, Millipore, MA, USA), followed by washing with PBS twice. The isolated exosomes were identified by transmission electron microscope (JEM-1200EX, Tokyo, Japan), nanoparticle tracking analysis (NTA) (NanoSight NS300, Worcestershire, UK), and flow cytometry (Accuri Cytometers, MI, USA).

Exosome uptake assays

M2 macrophages-derived exosomes were labelled with a red fluorescent dye PKH26 (Cat# MINI26-1KT, Sigma-Aldrich, MO, USA) and added to human liver stellate cells in culture (LX2) for 0, 3, 6, 24 hours. Hoechst dye (Cat# PH0528, Phygene, Fuzhou, P. R. China) was used to detect the nuclei, the uptake of exosomes by LX2 cells was analysed using an inverted fluorescence microscope (Leica DMI8, Wetzlar, Germany).

Western blotting

Total proteins were extracted from cells using radio-immunoprecipitation assay (RIPA) buffer (Cat# 89900, Thermo Fisher Scientific Inc., MA, USA) supplemented with protease inhibitor and phosphatase inhibitor cocktail (Cat#78440, Thermo Fisher Scientific Inc., MA, USA). The protein lysate was subjected to 8–10% sodium dodecyl sulphate polyacrylamide gel electrophoresis (SDS–PAGE), transferred onto a polyvinylidene fluoride (PVDF) membrane, and incubated with antibodies against Tubulin (diluted 1:1000, Cat# 2128, Cell Signaling Technology, MA, USA), αSMA (diluted 1:1000, Cat# ab32575, Abcam, MA, USA), COL1A1 (diluted 1:1000, Cat# ab138492, Abcam), and COL3A1 (diluted 1:1000, Cat# ab184993, Abcam) at 4°C overnight. For detection, an HRP-conjugated secondary antibody (diluted 1:10000, Cat# ab6721, Abcam) and the Enhanced Chemiluminescence (ECL) detection system were used.

RNA extraction and quantitative reverse transcription PCR

Total RNA was isolated using TRIzol (Cat# 15596018, Invitrogen, CA, USA) according to manufacturer's instructions. Real-time PCR was performed with the TB Green Premix Ex TaqII (Cat# RR820A, Takara, Kyoto, Japan) on a LightCycler 480 system (Roche, Basel, Switzerland). The expression of target mRNAs was normalized with *Gapdh* or *β-actin* while that of microRNAs was normalised with snRNA U6. The fold changes were calculated using $2^{-\Delta\Delta CT}$ method. The sequences of the primers are enlisted in Table S1.

Flow cytometry

Flow cytometry was performed for examining the surface marker expression on M2 macrophages. Briefly, the cells were stained with PE-conjugated anti-CD86 (Cat# 12-0869-42, eBiosciences, CA, USA) or APC-conjugated anti-CD206 (Cat# 17-2069-42, eBiosciences, CA, USA) in the dark at room temperature for 30 min. Subsequently, the cells were washed with PBS supplemented with 2% FBS, and the percentage of $CD86^{+}$ cells—identified as M1 macrophages, the percentage of CD206+ cells—identified as M2 macrophages—were analysed by flow cytometer. The raw data was analysed by CytExpert software 2.3.

Histopathology and immunohistochemistry studies

The paraffin sections were then dehydrated and stained with haematoxylin and eosin or Masson stains. For the Oil Red O staining, fresh liver tissues were snap-frozen in liquid nitrogen and their frozen sections were prepared. The frozen sections were subsequently stained with Oil Red O and counterstained with haematoxylin.

For the immunohistochemical staining, paraffin sections were subjected to antigen retrieval and blocking post deparaffinization and subsequent rehydration. The sections were then incubated with antibodies against αSMA and CD163 at 4°C overnight, followed by incubation with an HRP-conjugated secondary antibody (diluted 1:200, Cat# GB23303, Servicebio) at room temperature for 50 min. Finally, the tissue sections were stained with a DAB (Cat# G1211 Servicebio) staining solution and counterstained with haematoxylin. The brown positive staining area was quantified using NIH-ImageJ software.

Immunofluorescence analysis

For the immunofluorescence analysis, the cells were fixed with 4% paraformaldehyde, permeabilized with 0.5% Triton-X-100 (Cat# T9284, Sigma-Aldrich), and blocked with 5% BSA (Cat# G1211 Servicebio) for 30 min. The cells were then incubated with antibodies against αSMA at 4°C overnight, followed by incubation with fluorophore conjugated secondary antibody at room temperature for 1 hour. Finally, the nuclei were stained with Hoechst and the images were captured using an inverted fluorescence microscope (Leica DMI8, Wetzlar, Germany).

Dual-luciferase reporter assay

The psiCHECK 2.0 luciferase vector was used for the luciferase reporter assays. Briefly, the wild type or mutant *CAMSAP1* 3′ UTR plasmids and wild type or mutant *PUM1* 3′ UTR plasmids were co-transfected with miR-411-5p mimic/inhibitor/controls into the HEK293 cells. Subsequently, the firefly and *Renilla* luciferase activities were measured by adding the Luciferase Assay Reagent to the transfected cell lysates. The relative luciferase activities were then calculated as the ratio of firefly to *Renilla* luciferase luminescence.

QUANTIFICATION AND STATISTICAL ANALYSIS

The data are expressed as the mean ± standard error of mean (SEM) and were analysed using GraphPad Prism 8.0 (GraphPad Software Inc., La Jolla, CA). Student's t-test was used to compare the mean of two samples while one-way ANOVA was performed for multiple comparisons. Correlation was assessed by linear regression analysis and the Pearson's correlation coefficient. p values less than 0.05 were considered statistically significant.